

# The Interaction of Type Ia Supernovae with their Surroundings: The Exponential profile in 2D

Vikram V. Dwarkadas

RCfTA, School of Physics, A28 Univ of Sydney, NSW 2006, Australia

Received \_\_\_\_\_; accepted \_\_\_\_\_

## ABSTRACT

The evolution of Type Ia supernovae in the surrounding medium is studied using 2-dimensional numerical hydrodynamic simulations. The ejecta are assumed to be described by an exponential density profile, following the work of Dwarkadas & Chevalier (1998). The case of a circumstellar region formed by mass loss from the progenitor or a companion star is also considered. The decelerating contact discontinuity is found to be Rayleigh-Taylor (R-T) unstable, as expected, and the nature of the instability is studied in detail for 2 cases: 1) a constant density ambient medium, and 2) a circumstellar medium whose density goes as  $r^{-2}$ . The nature of the instability is found to be different in both cases. In the case of a circumstellar medium the instability is much better resolved, and a fractal-like structure is seen. In the case of a constant density medium the extent of growth is less, and the R-T fingers are found to be limited by the presence of Kelvin-Helmholtz mushroom caps at the tips of the fingers. The unstable region is far enough away from the reverse shock that the latter is not affected by the mixing taking place in the interaction region. In contrast the reverse shock in the case of a circumstellar medium is found to be rippled due to the formation of instabilities. In neither case is the outer shock front affected. These results are consistent with similar studies of power-law ejecta profiles conducted by Chevalier, Blondin & Emmering (1992). Our results are then applied to Tycho’s supernova remnant. We conclude that it is unlikely that the instabilities seen in recent radio images of the remnant are similar to those studied herein, although we do not discount the possibility of initial conditions different from those studied herein leading to a much larger growth than we see in our simulations. We suggest that such instabilities may be better observed at X-ray wavelengths which probe the high-density shocked ejecta region.

*Subject headings:* hydrodynamics — instabilities — shock waves — supernova  
remnants — supernovae: individual (SN 1572)

## 1. INTRODUCTION

The evolution of supernova remnants (SNRs) has been classically assumed to go through 4 stages (see for example Woltjer 1972). In the initial free-expansion or ejecta-dominated stage, the expansion of the remnant is determined by the properties of the supernova ejecta and the density of the surrounding medium. The mass of the ejected material, the kinetic energy of the explosion, the density profile of the ejected material and the density distribution in the ambient medium are all required to understand the expansion of the remnant in this stage. This phase is particularly important because many of the so-called “historical” supernovae (SNe) known in our galaxy may either be in this stage, or be making a transition from it to the Sedov or adiabatic phase, where the mass swept-up by the SN shock wave substantially exceeds the ejecta mass.

Determination of the density profile of the ejected material is not a simple task, and little observational evidence is available. The density depends on the structure of the progenitor star and the shock acceleration of the gas during the explosion (Chevalier & Fransson 1994). The best available information is for SN 1987A, where the density seems to be well constrained by models of the explosion (eg. Arnett [1988] and Shigeyama & Nomoto [1990]). In this case the density in the outer parts of the ejecta in the free-expansion phase varies approximately as a power-law with velocity. Similar models have been used to describe Type II SNe in general, and self-similar solutions for power-law ejecta interacting with a power law or constant density surrounding medium have been derived by Chevalier (1982a) and Nadozhin (1985). Recently, Truelove & McKee (1999) have presented more general approximate solutions for the evolution of non-radiative SNRs in the ejecta-dominated stage. The special case of interaction of a uniform density ejecta with the surrounding medium will also be addressed in Drury and Dwarkadas (2000).

Power-law models (with an exponent of 7) have also been used to describe the ejecta

density profile in Type Ia SNe (Chevalier 1982a, 1982b; Fabian, Brinkmann & Stewart [1983], Band & Liang [1988]), which are believed to result from the degenerate ignition of a C/O white dwarf in a binary system. However Dwarkadas & Chevalier (1998, hereafter DC98) showed that an exponential ejecta profile for Type Ia SN explosions gives the best fit to the density profile. Furthermore, they compared the interaction of Type Ia SNe described by power-law, exponential and constant density ejecta profiles with the surrounding medium, in the simplest case of spherical symmetry.

This paper expands on the work of DC98, presenting high-resolution two-dimensional simulations of ambient medium interaction in Type Ia’s using an exponential density profile to describe the ejecta. We compare the properties of the two-dimensional flow to that in one-dimension. The 2D grid allows us to investigate the multi-dimensional aspects of the flow, especially the formation of hydrodynamic instabilities in the free-expansion phase. In particular we study the evolution and growth of the Rayleigh-Taylor (R-T) instability that arises at the decelerating contact discontinuity.

The role of the R-T instability in young supernova remnants has been receiving great attention in recent years (see Chevalier 1996). The accumulation of observational evidence of substantial non-radial motions and mixing occurring in the explosion of SN 1987A led several groups to perform multi-dimensional simulations of supernova explosions (Arnett et al. 1989; Benz & Thielemann 1990; Fryxell et al. 1991; Herant & Benz 1991). Hydrodynamic instabilities in self-similar driven waves were investigated by Chevalier, Blondin & Emmering (1992, hereafter CBE92). The presence of instabilities can lead to fragmentation and the formation of clumps or blobs in the interface between the ejecta and the surrounding material. Mixing among various layers can destroy any early stratification and cause certain elements to be found at larger radii than would otherwise be expected. In this paper our aim is to characterise the nature and growth of these instabilities for the case

of SN ejecta described by an exponential density distribution. Implications of mixing of the ejecta and circumstellar (CS) material for the observable supernova remnants, in particular Tycho’s SNR (SN1572), is also addressed. The growth of these instabilities under various conditions is investigated, such as a constant density medium (indicative of the interstellar medium) or a circumstellar medium formed by mass loss from the progenitor star. We compare and contrast the results in these two cases.

The rest of this paper proceeds as follows. In §2 we first review briefly the properties of an exponential ejecta density profile. This is followed by initial results of the 2D simulations in §3. In §4 we discuss the R-T instabilities in more detail. §5 focuses on the application of our results to Type Ia SNe, especially Tycho’s SNR, while §6 contains a brief discussion and summary.

## 2. The Exponential Ejecta Profile

The exponential profile used to describe the SN ejecta can be written as (DC98):

$$\rho_{SN} = A \exp(-v/v_e) t^{-3} \quad (1)$$

where, by integrating over the total ejecta distribution, taken to have mass  $M_e$  and kinetic energy  $E$ , we find that

$$v_e = \left[ \frac{E}{6M_e} \right]^{1/2} = 2.44 \times 10^8 E_{51}^{1/2} \left[ \frac{M_e}{M_{ch}} \right]^{-1/2} \text{ cm s}^{-1}, \quad (2)$$

where  $M_{ch} \equiv 1.4 M_{\odot}$  is approximately the Chandrasekhar mass, and  $E_{51}$  is the explosion energy in units of  $10^{51}$  ergs. The value of  $E_{51}$  quoted in the literature lies anywhere between about 0.3 and 1.8. The parameter  $A$  is given by:

$$A = \frac{6^{3/2}}{8\pi} \frac{M_e^{5/2}}{E^{3/2}} = 7.67 \times 10^6 \left[ \frac{M_e}{M_{ch}} \right]^{5/2} E_{51}^{-3/2} \text{ g s}^3 \text{ cm}^{-3} . \quad (3)$$

The interaction of the SN ejecta with the ambient medium gives rise to a double shocked structure, consisting of a forward shock expanding into the surrounding medium, and a reverse shock that moves inward in a Lagrangian sense, separated by a contact discontinuity. We have carried out 2-dimensional hydrodynamic simulations of the supernova ejecta colliding with the ambient medium. The assumption of spherical symmetry with regard to the exponential ejecta density distribution is certainly an approximation. In reality the formation of instabilities during the explosion will probably destroy any such early symmetry, leading to large-scale, possibly turbulent convective motions (Müller 1998). Nevertheless, this assumption is a valid starting point for such a study, and the inclusion of clumps and non-radial flows would be the subject of future, more complicated studies (see Wang & Chevalier 2000)

Our lack of knowledge of the progenitors of Type Ia SNe (eg. Livio 1999) makes it unclear what the density structure is in the immediate surroundings. The lack of radio and X-ray emission, and of nebular excitation lines from circumstellar interaction, points to a medium of constant low density. However if Type Ia’s are formed from degenerate ignition in a white dwarf, then it is clear that the white dwarf must be in a binary system, and mass transfer must be occurring (Wheeler 1996). A circumstellar region due to mass loss from the secondary star would then be expected, although its extent may be small. Cumming et al. (1996) place limits on the properties of such a region. In this paper we consider both cases, that of a constant density surrounding medium and a circumstellar medium. If the mass loss rate and velocity of the wind from the companion star are constant, the density of the circumstellar medium (CSM) decreases inversely as the square of the radius. The supernova remnant will remain in such a medium only for a few decades at most.

Nevertheless, as shown by DC98, the passage of the shock wave through such a CS region can leave an impression on the density structure of the interaction region even after the shock wave has exited the CS region. Thus it is both observationally relevant as well as academically interesting to study the evolution of the shock within a circumstellar medium. Furthermore, while an exponential profile has at present been postulated only in relation to Type Ia SNe, it must be emphasised that it is really not clear what the structure of the ejecta density profile is for any supernova other than possibly SN 1987A, despite recent progress in this direction (see for instance Matzner & McKee [1999]). A detailed study of the exponential ejecta density expanding into various ambient media is thus warranted.

### 3. 2D Simulations

The simulations were carried out using the VH-1 code, a 3-Dimensional finite-difference hydrodynamic code based on the Piecewise Parabolic Method (Colella and Woodward 1984), written by the Virginia Hydro group. The code, obtained from Dr. John Blondin at NCSU, solves the equations of conservation of mass, momentum and energy in Lagrangian co-ordinates, and then remaps the variables back to the original Eulerian grid. It has been extensively tested on various astrophysical hydrodynamical problems. The version employed here uses an expanding grid that tracks the outer shock front and expands along with it, making it ideally suited to problems where the dimensions change by many orders of magnitude over the course of the run.

The evolution of the outer shock front in 2D is similar to that in 1D, as described by DC98. One important quantity is the evolution of the expansion parameter with time. If the radius is proportional to time raised to some power ( $R \propto t^\delta$ ), then  $\delta$  is the expansion parameter. This is a dimensionless quantity that can be used to discriminate between the various phases of remnant evolution. In Figure 1 we show the evolution of the expansion



parameter with time for a Type Ia SN evolving in a constant density medium. The time axis is normalised to the quantity  $T' \approx 248 E_{51}^{-0.5} \left( \frac{M_e}{M_{ch}} \right)^{5/6} n_0^{-1/3}$  yr using equation (4) in DC98. The number density  $n_0$  is related to the ambient medium density  $\rho$  by  $n_0 = \rho / 2.34 \times 10^{-24} \text{ cm}^{-3}$ , appropriate for a medium with a H/He ratio of 10:1. In Figure 2 we show the same plot for a CS medium whose density decreases as  $r^{-2}$ . In this case the time normalisation is taken to be  $T'_2 = E^{-0.5} M_e^{1.5} D^{-1}$ , where  $D = \rho r^2$ . These plots show how the expansion parameter varies over the evolution of the remnant in the free expansion phase, until it reaches the Sedov value, which is 0.4 in the case of the constant density medium and 0.67 in the case of a circumstellar medium. The continuous evolution of the expansion parameter is consistent with the higher-resolution 1D calculations of DC98.

As the outer shock expands into the circumstellar medium, it begins to sweep up the ambient material. The Sedov value of the expansion parameter in either case is reached only once the swept-up mass significantly exceeds the ejecta mass, by a factor of 30 or more. However, once the mass of swept-up material becomes comparable to the ejecta mass, the pressure of the surrounding medium causes the SN ejecta to decelerate. As the mass of shocked ambient material continues to increase, the reverse shock begins to move inwards towards the center, and the contact discontinuity between the two shocks begins to decelerate. The high density shocked SN ejecta behind the contact discontinuity are decelerated by the swept-up material ahead of it. The pressure and density gradients lie in opposite directions, and the system becomes unstable to Rayleigh-Taylor (R-T) instabilities. Small-amplitude perturbations, with wavelength on the size of a few grid zones, then occur. The size of these perturbations appears to grow linearly, and soon the familiar R-T fingers spread out into the shocked surrounding medium. The tips of these fingers terminate in bulbous-shaped mushroom-like heads, a result of the Kelvin-Helmholtz instability as the shocked gas surrounding the fingers tries to slide past them. This evolution is depicted in Figures 3 and 4, which are discussed in detail below.

#### 4. The Rayleigh-Taylor instability

The Rayleigh-Taylor instability arises at the interface between a low-density fluid supporting a high-density fluid (e.g. Chandrasekhar 1961). In our case the analogous situation arises at the contact discontinuity separating the shocked SN ejecta from the shocked ambient medium, as described above. Small ripples arise initially along the entire length of the contact discontinuity. No explicit perturbation is required to induce the instability, which can be triggered purely by the numerical noise in the system. We have also tested the case when explicit perturbations of various amplitudes are introduced (§4.2). The ripples in our higher resolution simulations appear to start off close to the symmetry axis and then move towards the equator, but this is not easily confirmed, since by the time the ripples acquire an appreciable amplitude they are spread over the entire contact discontinuity. It is however quite likely that approximations at the boundary lead to minor fluctuations that trigger the instability.

Figure 3 shows grey-scale images of the evolution of the instability with time, for a SN evolving in a constant density medium, which we refer to henceforth as Case 1. Figure 4 shows the same for a Type Ia SN evolving in a circumstellar medium, referred to as Case 2. The times listed for each plot are normalised in the same manner as for the expansion parameters (§3). The radius for Case 1 is normalised to the value  $R' = \left(\frac{M_e}{\frac{4}{3}\pi\rho}\right)^{1/3} \approx 2.19 \left(\frac{M_e}{M_{ch}}\right)^{1/3} n_0^{-1/3}$  pc. For Case 2 the radius normalisation is  $R' = M_e/D$ , where  $D = \rho r^2$ . The growth of the finger size (the penetration of the denser layer into the less dense layer) with time for Case 1 is shown in Figure 5. The plot for Case 2 looks quite similar when normalized to the appropriate units and is not shown.

Theory predicts that the size of the R-T fingers should increase as the square of the time. However a simple quadratic fit was found to be inadequate to model the growth, while a second order least-squares polynomial fit was found to provide a reasonable solution. The

deviations are much larger earlier on, which is partly due to our inability to determine the amplitude of the perturbation in the very early stages. The fact that a linear as well as a quadratic component is needed is consistent with the fact that the flow is not self-similar (eg. Dalziel et al. 1999).

A standard linear analysis of the R-T instability shows that the growth rate is proportional to the square-root of the wavenumber (eg. Chandrasekhar 1961; Sharp 1984). According to this the smallest wavelengths should be the most unstable. In our simulations we find that the initial ripples are on the scale of a few (5-10) grid zones. Smaller wavelengths are damped by any inherent viscosity in the numerical method. The ripples grow into spike-like protrusions, forming the characteristic Rayleigh-Taylor ‘fingers’. As the spiky protrusions expand outwards into the surrounding medium, the shocked ambient material tries to slide past them. This gives rise to shear flow at the edges, leading to the growth of Kelvin-Helmholtz (K-H) instabilities, visible as the bulbous, mushroom-shaped heads on the R-T fingers. The flow of the shocked ambient medium past the fingers also tends to limit their growth, more so in the constant density medium case. Over time the fingers appear to merge into one another and the fastest growing wavelength increases with time, or correspondingly the number of individual R-T fingers seen decreases with time. The scale of the fastest-growing wavelength is set by the system, independent of the initial perturbation that triggered the instability. The result is that as the reverse shock approaches the center, the unstable wavelength, or alternatively the number of R-T fingers seen, is the same no matter what the amplitude of the initial perturbation, or even if no initial perturbation was applied to the system.

All our simulations show a jet-like structure along the symmetry axis. This structure is even more prevalent in those simulations where an initial perturbation was introduced. When the jet breaks through the outer shock it tends to “fan out”, thus giving rise to a large

mushroom-shaped cloud. These structures, prevalent in many other numerical simulations embodying the same symmetry, are most likely numerical artifacts and are not real. They are formed at the symmetry axis, where the geometry results in grid zones whose volume is very small. Any fluid component perpendicular to the axis of symmetry (i.e. flowing into the axis) has nowhere to go and is deflected along the axis, thus resulting in these spurious structures.

We elaborate later on the differences between the instabilities seen in the constant density and the  $1/r^2$  surrounding medium, after first discussing the similarities between the two cases. A point to note in all our simulations is that, irrespective of the initial amplitude of the perturbation or of the nature of the surrounding medium, the unstable region never occupies more than about 50% of the interaction region. The size of the R-T projections grows faster than the size of the interaction region, so that the width of the mixing region tends to increase with time. However in all cases the reverse shock reaches the center, and the instabilities ceased to grow, when the mixing width was less than or about half the size of the interaction region. One implication of this is that the instabilities never penetrate the outer shock, and in fact have no direct effect on it. The appearance of the outer shock is not changed by the considerable amount of mixing occurring in the interaction region close to the contact discontinuity. The same is not true of the reverse shock in the circumstellar case, as described later.

While the above results are consistent with those found by CBE92 in their study of the Rayleigh-Taylor instability for power-law ejecta, a major difference exists between the two cases. The latter describe the quasi-steady evolution of the instability in the self-similar driven case, and in fact show (their Figure 7) how snapshots of the evolution taken at times two orders of magnitude apart hardly reveal any difference. The same is not true in the exponential case. Introduction of the velocity scale length in the exponential profile means

that the solution is no longer self-similar, even though it is scalable. The appearance of the unstable region tends to change, albeit slowly with time, and no two snapshots which are two decades apart in time resemble each other closely as in the models of CBE92.

A close look at Figures 3 and 4 shows that there is considerable difference between the growth of the instabilities in the two cases. In the constant density medium case the growth of the fingers appears stunted. The formation of the mushroom caps at the head of a finger tends to limit the growth of the projection. The projections grow to a much larger extent in the CS case, and occupy a greater fraction of the interaction region. We attribute these differences in large part to the difference in Atwood number between the two cases (eg. Sharp 1984). The Atwood number, or equivalently the density contrast between the shocked ambient and shocked ejecta material, governs the growth of the instabilities for small-amplitude perturbations of wavelength close to the critical wavelength required for unstable behaviour (Sharp 1984). The Kelvin-Helmholtz instability caused by the shocked fluid flowing past the spikes is more pronounced at lower values of the Atwood number, which is the case when the shock expands in a constant density medium. This can cause the caps to mushroom out, increasing the effect of the drag on the spike and slowing its growth. This difference in the two cases is similar to that seen by CBE92 in their study of R-T instabilities for self-similar driven waves.

The two cases are further differentiated by the effect of the instabilities on the reverse (inner) shock. In the constant density medium case, the contact discontinuity is far enough away from the reverse shock that the instabilities do not affect the shape of the shock, which stays smoothly spherical. However in the CS case the reverse shock is much closer to the contact discontinuity, and the pressure variations are higher, causing the reverse shock itself to get wrinkled. The corrugation of the inner shock (Figure 4, middle panels) occurs on a scale similar to the most unstable wavelength, and seems to get more pronounced as

the reverse shock heads towards the origin. Again, a similar effect was noticed by CBE92.

Note also that the time taken for the reverse shock to reach the centre in Figure 3 is about two-thirds of that found in the work of DC98. This is to be expected. The instabilities cause a “leakage” of pressure from the shocked ambient medium to the shocked ejecta. Thus the pressure driving the reverse shock is higher than in the spherically symmetric work of DC98, and the reverse shock consequently reaches the origin earlier.

The most likely scenario for supernova shock evolution is that it traverses a region of circumstellar medium followed by a constant density interstellar medium. As the shock moves from the CS to the constant density medium, the nature of the instabilities will change. The details will depend strongly on the extent of the CS region. If the size of the initial CS region is small, such that the instabilities do not have time to grow, then the effect of the CS region on the later evolution of the remnant is small. However we do find that in most cases the reverse shock remains corrugated even after the remnant is expanding primarily in a constant density medium. Thus, in addition to the spike in the density profile at the contact discontinuity, and the corresponding temperature drop mentioned in DC98, the shape of the reverse shock itself is affected by passage through an initial CS region. The presence of a CS shell at the interface between the two media was not taken into account and would further affect the evolution of the instabilities.

#### 4.1. Effect of Grid Resolution

The effects of grid resolution on the instabilities merits consideration. Increasing the resolution leads to the appearance of structure on smaller scales, as would be expected. In Case 2 the instabilities appear to clump together with a number of sub-fingers arising from each finger, instead of appearing as individual spikes. The turbulent mixing behaviour,

with vortices being formed close to the projecting fingers, causes individual fingers to be bent at an angle, producing structures resembling question marks. The stems show the usual Kelvin-Helmholtz mushroom caps due to shear flows around the edges. The number of R-T clumps that exist when the reverse shock reaches the center remains the same in all simulations, although the substructure in each clump continually increases. The appearance somewhat resembles a tree-structure, with higher resolution revealing more branches in the tree and more stems arising from the branches (see top panels in Figure 6). The pattern is fractal in nature, although the code is unable to resolve individual stems very well. The mixing width (the width of the region occupied by the instabilities) shows a definite increase of a few percent with resolution in the earlier stages of the instability. This may be partly due to the fact that as the shock expands outwards, individual structures are more easily discernible in a higher resolution simulation as the increase in the size of a grid zone is not as large as in a lower-resolution simulation. As the instabilities evolve the mixing width occupied by the unstable region becomes approximately constant.

In Case 1 a similar overall effect is visible. Simulations with a higher grid resolution lead to more R-T fingers being visible. As the simulation evolves the amount of substructure also increases, as would be expected. Also visible is an increase in the size of the K-H caps at the heads of the stems in the higher resolution cases. As before however, the simulations appear quite similar once the reverse shock nears the inner boundary, and the number of R-T fingers is more or less the same. No fractal structure is seen, in contrast to case 2, although the fingers are much better defined with an increase in the number of grid zones, as would be expected. Another effect is that the instabilities appear to start earlier as the spatial resolution increases. An increase in grid resolution by 50% leads to a decrease in the time when the ripples are first seen by about 20%. Also important is the fact that, as the growth rate is limited, a minimum resolution is required to capture the growth of the instabilities. This is consistent with the results of Fryxell et al. (1991) for SN 1987A. We

have found that even a  $300 \times 300$  run does not generate the instabilities till the reverse shock is close in to the centre of the explosion, and that a grid of at least 500 azimuthal zones is necessary to capture the instabilities in detail.

#### 4.2. Effect of initial perturbation

We have investigated the effect of adding an initial perturbation of various amplitudes. A sinusoidal perturbation of wavelength equal to the angular dimensions of the grid was added. Figure 6 shows snapshots at approximately the same epoch in time from various runs for Case 2. Two cases with no perturbation added but different resolutions are shown in the first row. The remaining frames show cases where a perturbation of the given amplitude was introduced, all with the resolution set to 500 by 500 zones. In general we find that for Case 2 the overall effect of small-amplitude perturbations ( $\lesssim 10\%$ ) is tiny, and the instabilities develop in almost the same way as they do in the case of zero initial perturbation. Initially the differences appear large, with the no-perturbation simulations showing a more homogeneous growth of projections whereas simulations with initial perturbations show fewer and more well-defined fingers. However the differences decrease as the reverse shock moves inwards, and in most cases the appearance of the unstable region looks quite similar by the time the reverse shock nears the inner edge of the grid. The effects of perturbations of amplitudes  $\gtrsim 15\%$  are more pronounced. There is an increase in the amount of small-scale structure to be seen, and the larger perturbation simulation presents a more clumpy appearance. A small increase in the mixing width accompanies the increase in the amplitude of the perturbation. It is evident from Figure 6 that the effects of higher resolution and introduction of a perturbation are not independent, in the sense that increasing the resolution has a similar effect to adding a perturbation. The higher resolution case with no perturbation is quite similar to the runs with an initial perturbation.



For Case I the effect of adding an initial perturbation is more pronounced, as shown in Figure 7. The inhomogeneous appearance of very small wavelength projections is replaced by individually discernible fingers. The projections seem to stretch out further, but their number has decreased. Thus, although there is a definite increase in the mixing width, the volume occupied by the instabilities remains about the same. Again the differences decrease as the simulation proceeds, although even when the inner shock is close to the center the differences are immediately perceptible, unlike in Case 2. Another distinction is that with the addition of an initial perturbation, the instabilities form much earlier than in the case of no perturbation, and a lower grid resolution is adequate to show that the instabilities are present, although a higher resolution grid is still required to resolve them. A grid with 300 azimuthal zones is sufficient to at least demonstrate the growth of the instabilities (Fig 7).

## 5. Tycho’s SNR (SN 1572)

Rayleigh-Taylor instabilities have been often cited as the cause of corrugations and rippled structure in images of SNRs. Velazquez et al. (1998) have studied the Rayleigh-Taylor instability in Tycho’s SNR, following up on VLA observations carried out by Reynoso et al. (1997). They conclude that wavy structure seen in the NE quadrant of the VLA image, formed by small, regularly spaced protrusions just behind the outer shock front, is due to Rayleigh-Taylor instabilities. It is unclear if the results of our work support such an interpretation. As emphasised in the previous section, in no case did the instabilities in our simulations cover more than half the interaction region, let alone penetrate the outer shock front, as do some of the protrusions shown in Figure 2 of Velazquez et al. (1998). If the radio emission is coming from just behind the outer shock our simulations imply that it is unlikely that any unstable structure should be visible close to the outer rim. Moreover, the calculations of DC98 and our own 2D calculations show that a tenable model

for Tycho requires that the reverse shock be quite far out, and the size of the interaction region be small. The instabilities will then still be in the incipient stages, as is also found by Velazquez et al. (1998). However that would mean that they would occupy an even smaller fraction of the interaction region, and would not likely be as prominent as they are in the radio images, unless some effect led to an increase in entropy within the mixing region, leading to a larger growth of the R-T instabilities than is observed in our simulations. The latter is not entirely improbable - it is possible perhaps that thermal instabilities in the surrounding medium, operating over evolutionary timescales, set up a very clumpy and non-linear initial condition for the growth of these instabilities, resulting in much larger growth than that studied herein. There exists also the possibility that if the NE portion is running into a high density H1 cloud as revealed by Reynoso et al. (1997), some of the corrugated shock structure may be due to interaction of the remnant with an uneven cloud boundary.

Based on the results of the simulations carried out herein, we may argue that emission which arises predominantly from just behind the outer shock is unlikely to reveal evidence of the R-T instabilities studied in this paper. However the instabilities might show up better in maps of emission from close to the interface between the shocked ambient and shocked ejecta gas. A case in point is again Tycho's SNR. X-ray line observations by Hwang and Gotthelf (1997) have provided narrow-band images in various emission lines, such as Si, S and Fe. These reveal a shell which is generally circular, but many of the images (their Figure 4e) show a corrugated, wavy outer shell and the presence of clumps. An isolated knot is also seen in several images near the southeast bulge. The presence of Si, S and Fe lines indicates that much of the emission is coming from the reverse-shocked ejecta material (see also Hwang et al. 1998). The Si and S emission may in fact be arising from close to the contact discontinuity (DC98). If so, the rippled outer boundaries may be a result of R-T instabilities similar to those described in this paper. We have carried out simulations

with parameters that may be reasonable for Tycho’s SNR. Although these simulations have not exhaustively explored the parameter space (and as such are not intended as a specific model for the remnant), they do indicate that instabilities would arise within a couple of hundred years after the explosion, and that, depending on the initial conditions, they would not yet have progressed into the non-linear phase at the age of Tycho’s SNR.

We could perhaps summarise by saying that for SNe with an exponential ejecta density profile in the free-expansion phase, the presence of instabilities near the contact discontinuity is more likely to be revealed in X-ray than in radio images. This implies a lack of correlation between the relative brightness of the radio and X-ray images, at various points around the circumference. Such a lack of correlation is seen in images of Tycho (Hwang and Gotthelf 1997).

## 6. Summary

We have carried out 2-dimensional simulations of Type Ia SNe interacting with the ambient medium, expanding on the work of DC98. An exponential density distribution was assumed for the ejecta. The simulations reveal that the decelerating contact discontinuity separating the shocked supernova ejecta from the shocked surrounding medium is unstable to Rayleigh-Taylor instabilities, as expected.

The nature and characteristics of the instabilities was examined. The instabilities tend to cover at most 50% of the interaction region. In no case is the outer shock affected by the turbulent mixing in the interior. However, if the surrounding medium is a circumstellar medium formed by mass loss from the companion star, then the reverse shock is found to be wrinkled due to the effect of the instabilities. The scale of the instabilities as they enter the non-linear regime is independent of the initial perturbations introduced into the system.

The effect of increasing resolution is to increase the small-scale structure visible in each R-T finger. A fractal-like pattern is seen for a surrounding CS medium, with multiple fingers forming an R-T clump. However the number of such clumps remains the same irrespective of the initial perturbation. If the ambient medium is of constant density, then the amount of substructure seen is greater, but no clear, well-defined fractal pattern is formed.

Our results suggest that corrugated outer shocks in SNRs cannot be attributed to instabilities of the type studied herein. We do caution however that this may be a result of the initial conditions assumed herein, and it is possible that different initial conditions, or a non-axisymmetric surrounding medium, could result in much larger growth of the R-T fingers. We feel that the instabilities are more likely to be visible in emission that arises from the reverse-shocked ejecta, such as X-ray emission from young supernova remnants. This is perhaps the case for Tycho’s SNR, and some of the clumpy structure seen in the images reported by Hwang and Gotthelf (1997) could possibly be a result of R-T instabilities.

The study of instabilities helps us to understand the multi-dimensional structure that is formed during the evolution of supernova remnants, and thereby aid in interpretation of the observational data. Further studies are required that take into account instabilities that may occur during or just after the explosion process, and determine how these affect the later evolution. Also, 3-dimensional studies often tend to show subtle differences from 2-dimensional ones, and a fuller understanding will require 3-dimensional simulations.

**Acknowledgements** I would like to thank Dr. Roger Chevalier and Dr. Lewis Ball for useful discussions and comments on the manuscript, Dr. Noella D’Cruz for a critical reading, and the anonymous referee for useful comments.

## REFERENCES

- Arnett, W. D. 1988, *ApJ*, 331, 377
- Arnett, W. D., Fryxell, B. A., & Müller, E. 1989, *ApJ*, 341, L63
- Benz, W., & Thielemann, F.-K. 1990, *ApJ*, 348, L17
- Band, D. L., & Liang, E. P. 1988, *ApJ*, 334, 266
- Chandrasekhar, S. 1961, *Hydrodynamic and Hydromagnetic Stability*, (Oxford: Clarendon Press)
- Chevalier, R. A. 1982a, *ApJ*, 258, 790
- Chevalier, R. A. 1982b, *ApJ*, 259, 302
- Chevalier, R. A. 1996, in *The Interplay Between Massive Star Formation, The ISM and Galaxy Evolution*, eds. D. Kunth, B. Guiderdoni, M. Heydari-Malayeri, & Trinh Thuan, (Cedex: Editions Frontieres), 151
- Chevalier, R. A., & Fransson, C. 1994, *ApJ*, 420, 268
- Chevalier, R. A., Blondin, J. M., & Emmering, R. T 1992, *ApJ*, 392, 118 [CBE92]
- Colella, P., & Woodward, P. R. 1984, *J. Comp. Phys.*, 54, 174
- Cumming, R. J., Lundqvist, P., Smith, L. J., Pettini, M., King, D. L. 1996, *MNRAS*, 283, 1355
- Dalziel, S. B., Linden, P. F., & Youngs, D. L. 1999, in *the Fifth International Workshop on the Physics of Compressible Turbulence*
- Drury, L. O’C, & Dwarkadas, V. V. 2000, in preparation

- Dwarkadas, V. V., & Chevalier, R. A. 1998, *ApJ*, 497, 807 [DC98]
- Fabian, A. C., Brinkmann, W., & Stewart, G. C. 1983, in *Supernova Remnants And Their X-Ray Emission (IAU Symposium #101)*, ed. J. Danziger and P. Gorenstein, (Dordrecht: D Reidel), 119
- Fryxell, B., Müller, E., & Arnett, W. D. 1991, *ApJ*, 367, 619
- Herant, M., & Benz, W. 1991, *ApJ*, 370, L81
- Hwang, U., & Gotthelf, E. V. 1997, *ApJ*, 475, 665
- Hwang, U., Hughes, J. P., & Petre, R. 1998, *ApJ*, 497, 833
- Livio, M. 1999, to appear in *Type Ia Supernovae: Theory and Cosmology* [Cambridge University Press], in print
- Matzner, C. D., & McKee, C. F. 1999, *ApJ*, 510, 379
- Müller, E. 1998, in *Computational Methods for Astrophysical Fluid Flow*, eds. LeVeque, Mihalas, Dorfi and Müller, (Berlin: Springer-Verlag), 343
- Nadozhin, D. K. 1985, *ApSS*, 112, 225
- Reynoso, E. M., Moffett, D. A., Goss, W. M., Dubner, G. M., Dickel, J. R., Reynolds, S. P., & Giacani, E. B. 1997, *ApJ*, 491, 816
- Sharp, D. H. 1984, *Physica*, 12D, 3
- Shigeyama, T., & Nomoto, K. 1990, *ApJ*, 360, 242
- Truelove, J. K., & McKee, C. F. 1999, *ApJS*, 120, 299
- Velazquez, P. F., Gomez, D. O., Dubner, G. M., Gimenez de Castro, G., & Costa, A. 1998, *A&A*, 334, 1060

Wang, C.-Y., & Chevalier, R. A. 2000, in preparation

Wheeler, J. C. 1996, in *Evolutionary Processes in Binary Stars* (NATO ASI), ed. R. A. M.

J. Wijers, M. B. Davies & C. A. Tout, (Dordrecht: Reidel), 307

Woltjer, L. 1972, *ARAA*, 10, 129

## Figure Captions

Fig. 1.— Evolution of the expansion parameter with time, for a SNR evolving in a constant density medium. The X-axis denotes time in normalised units (see text). The expansion parameter is calculated after every 20 timesteps rather than being averaged over, leading to somewhat large fluctuations in this and the next figure. The evolution proceeds until the reverse shock is close to the center and the expansion parameter approaches the Sedov-Taylor value of 0.4, appropriate for a constant density ambient medium.

Fig. 2.— Evolution of the expansion parameter with time, for a SNR evolving in a circumstellar medium. The X-axis denotes time in normalised units (see text). The evolution proceeds until the reverse shock is close to the center and the expansion parameter approaches the Sedov-Taylor value of 0.67, appropriate for an ambient medium whose density decreases as  $r^{-2}$ .

Fig. 3.— Density snapshots from a 500 X 500 run for a Type Ia SNR evolving in a constant density medium. No initial perturbation was applied. The size scale of the grid and the time at which each plot is depicted are listed on each image, in terms of the scaling variables described in the text. The shading is such that lighter colour represent higher densities. The innermost and outermost black regions do not constitute a part of the grid.

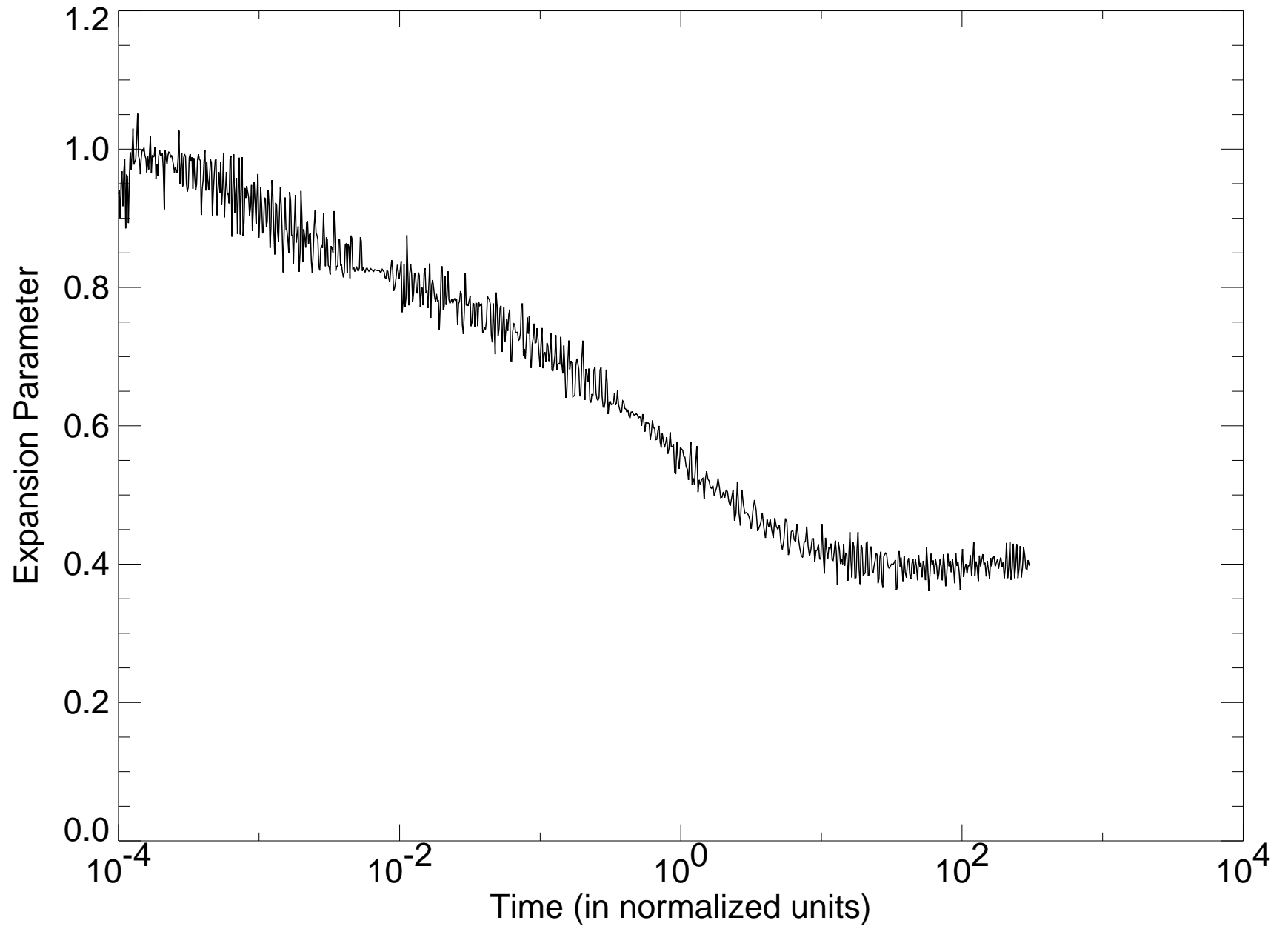
Fig. 4.— Density snapshots from a 500 X 500 run for a Type Ia SNR evolving in a CSM with density decreasing as  $r^{-2}$ . No initial perturbation was applied. The size scale of the grid and the time at which each plot is depicted are listed on each image, in terms of the scaling variables described in the text. The shading is similar to that in the previous image.

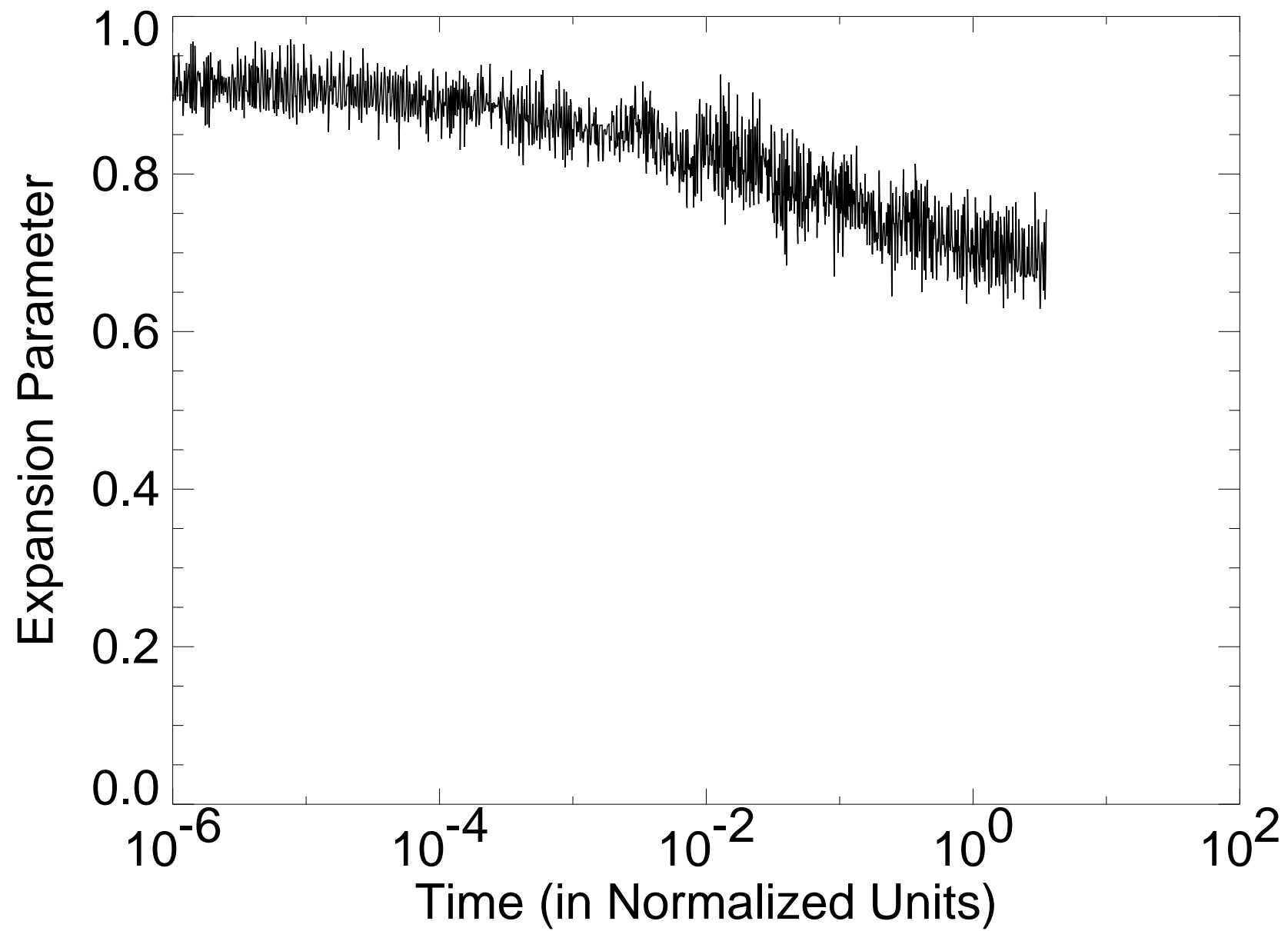
Fig. 5.— A plot of the size of the R-T fingers versus (normalised) time. The dashed line represents a second-order polynomial fit.



Fig. 6.— Density snapshots, at approximately the same epoch, from various runs for case 2. The top row includes two runs with different grid resolutions without the addition of an initial perturbation. The other runs included an initial perturbation of different amplitudes, as labelled, with a  $500 \times 500$  zones resolution.

Fig. 7.— Density snapshots, at approximately the same epoch, from three different runs for case 1. The leftmost image is from a run where no initial perturbations were introduced. The latter two included an initial perturbation but differ in grid resolution.



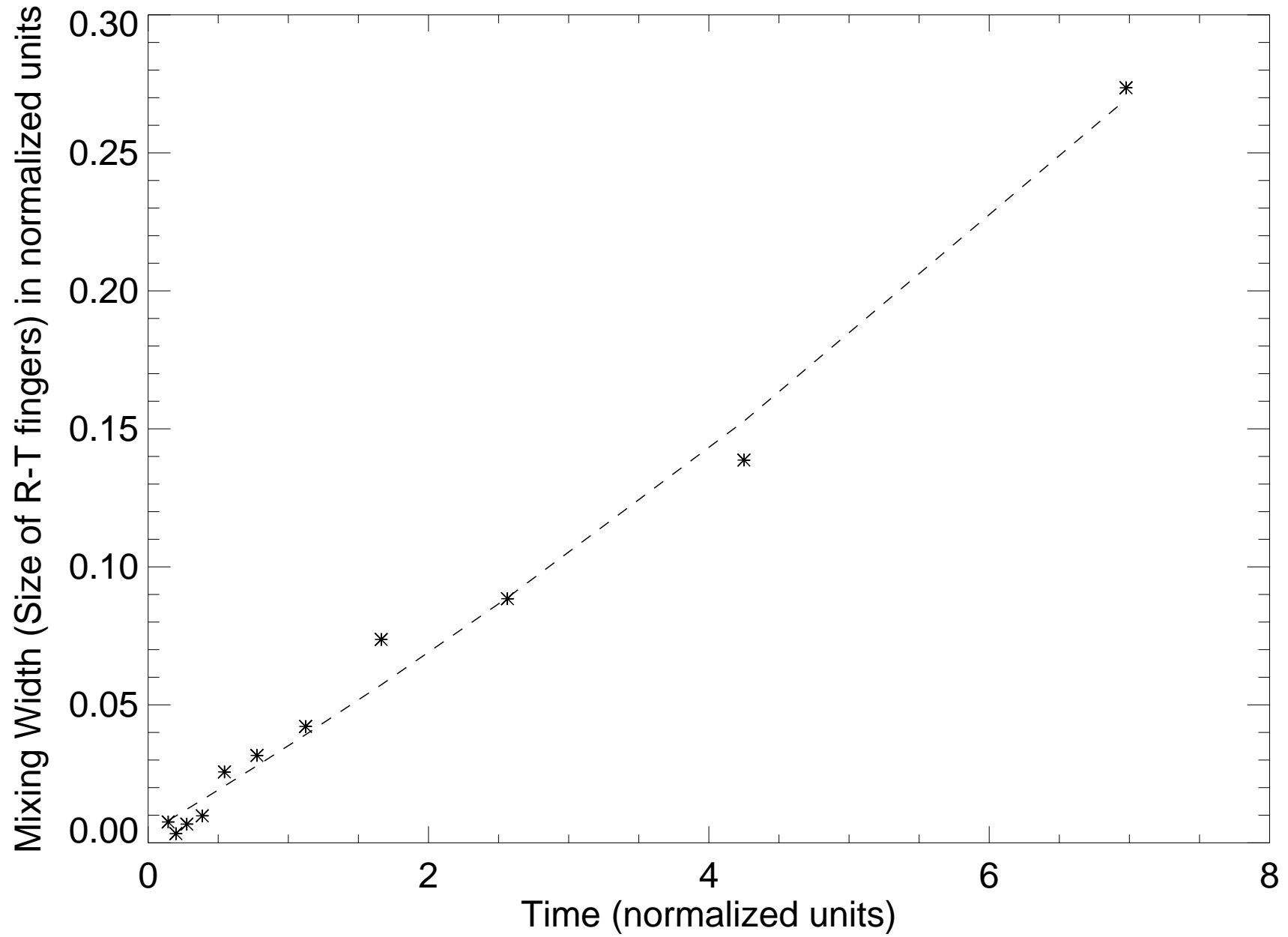


This figure "vikram-fig3.jpg" is available in "jpg" format from:

<http://arxiv.org/ps/astro-ph/0008076v1>

This figure "vikram-fig4.jpg" is available in "jpg" format from:

<http://arxiv.org/ps/astro-ph/0008076v1>



This figure "vikram-fig6.jpg" is available in "jpg" format from:

<http://arxiv.org/ps/astro-ph/0008076v1>

This figure "vikram-fig7.jpg" is available in "jpg" format from:

<http://arxiv.org/ps/astro-ph/0008076v1>